Segmentation-less digital rock physics using different effective medium theories

Eric J. Goldfarb*, Ken Ikeda, and Nicola Tisato, The University of Texas at Austin, Jackson School of Geosciences.

Summary

Micro computed tomography (µCT) is an effective way to obtain rock digital models that can be used, along with digital rock physics (DRP), to calculate rock properties. However, DRP has yielded mixed success that are in part due to limitations and uncertainty introduced by the segmentation processing method. Lately, segmentation-less DRP has been put forward potentially enabling DRP to become an avenue to inexpensively calculate rock properties. Ideally, DRP could be applied to an infinite number of samples such as drill cuttings. Here we present an investigation about effective medium theories that in segmentation-less DRP are the basis to assign properties to digital models. We compared a classic segmentation model with modifications of the Hashin-Shtrikman upper bound, and modifications of the Voigt-Reuss-Hill bound. The elastic property matrices that we obtain with these effective medium theories are used as models to simulate the propagation of ultrasonic waves. All effective medium theories applied to the rock as a whole significantly over predicted P wave velocity from 23% to 75%. Segmentation predicted a velocity 64% higher than the lab measurement. In all scenarios, the segmentation-less method predicts wave speeds more accurately than segmentation or their respective whole rock based DRP. For instance, a modification of the Voigt-Reuss-Hill bound yields a P wave velocity within 2% of that measured in the laboratory, while a modification of the Hashin-Shtrikman bound is within 19%.

Introduction

Recent trends have shown the need for deeper extraction of water, oil and gas (both conventional and otherwise), base metals, and precious metals (Catinat, 2010). Accessing geology of interest is difficult, rare, and expensive; thus subsurface model are often created from a few scraps of drill cuttings which increases model uncertainties (Horserud, 2001). When physical cores are obtained from deep wells, imaging with microscopy, assessing pore size distribution for porosity, and measuring permeability represent invasive and physically damaging operations for these samples. Furthermore, measuring elastic moduli require regular sample shapes (e.g., cylinders) that prove difficult to obtain and to preserve during extraction (Dvorkin et al, 2003).

Digital Rock Physics (DRP) is a method that employs X-ray micro-computed tomography (µCT) datasets as models to numerically simulate tests that are typically conducted in a laboratory. Moreover, DRP can be performed regardless the sample shape, and without damaging the sample. Micro

computed tomography (µCT) is increasing in popularity as a method to image and digitize the internal structure of rock samples (Espinoza et al., 2016). µCT records X-ray attenuation coefficients in a µCT-imagery that can be represented as a three dimensional matrix. This matrix physically represents the rock in real space. The model is composed of three dimensional cubic pixels, known as voxels, each one defined by a X-ray attenuation value or a unitless CT number.

Effective Medium Theory (EMT) allows estimating rock physical properties given a certain initial set of information such as density and porosity. To perform DRP, µCT imagery must be translated into physical property matrices. Typically, this is done through segmentation, i.e., by assigning to each voxel the physical properties of a pristine mineralogical phase or a pure fluid. Thus, segmentation tends to obliterate information such as the presence of cracks inside grains or the properties of grain contacts. As a consequence, with segmentation, the highest available resolution is required to fully represent a rock. This is problematic; for example, a scan with a resolution of 1 µm becomes computationally difficult to process, as it is terabytes in size when the physical sample is only ~1 cm^3 (Madonna et al., 2013).

By using segmentation based DRP, Madonna et al. (2012) calculated the effective elastic properties of a Berea Sandstone sample. They only obtained precise estimates of wave speeds by reconstructing grain to grain contacts and assigning to them arbitrary physical properties. With no grain reconstruction, Madonna et al. over predicted P wave velocity by ~100%. In other words, to be effective, grain-to-grain contacts and compliant porosity (i.e., cracks) should be imaged, implying that this method would perform even more poorly at lower resolutions.

The relationship between density, pore size distribution, and CT number has been noticed and used by several authors (e.g., Taud et al., 2004; Tanaka et al., 2011; Dunsmuir et al., 2006). Tisato and Spikes (2016) proposed a segmentation-less approach to assign voxel properties to CT imagery. As a first approximation, X-ray attenuation coefficient can be considered directly proportional to density (Beer, 1852; Landis and Keane, 2010). Thus, a CT-number to density calibration curve can be established when targets of known density are scanned along with the sample. Tisato and Spikes (2016) also used a simple linear relationship to translate density matrices into porosity matrices. They used the modified upper Hashin-Shtrikman bound (MHS) (Hashin and Shtrikman, 1962) to convert porosity to bulk

Choosing an Effective Medium for Digital Rock Physics with Micro Computed Tomography

and shear moduli and, as a consequence, to wave speeds. Finally, they propagated ultrasonic waves in two dimensional velocity models to calculate effective wave speeds. Their results compared reasonably well with laboratory measurements (i.e., ~4% over prediction).

The purpose of this paper is threefold: to demonstrate that the method of Tisato and Spikes can be applied on three dimensional (3D) matrices, that it can be applied successfully on a different sample, and to investigate how the chosen effective medium theory, which is used to translate porosity into elastic properties, affects the final result. To achieve such a goal we performed 7 wave propagation simulations using different EMTs.

Materials and Methods

A Berea Sandstone plug of 3.7 cm in length and 1.2 cm in diameter was scanned with μCT, at a resolution of 40 micro metres per voxel. The sample was mounted in the ERDμ pressure vessel, and scanned with the GE Phoneix v|tome|x at the University of Toronto (Tisato et al., 2014). The sample was rotated in 1080 equally spaced sectors totaling a 360 degree rotation. At each angle step, five 16 bit resolution projections were acquired with a X-ray energy of 120 keV. The software Phoenix X-ray datos—x-was used to produce slices from the 1080 projections. The dataset was corrected for beam hardening, automatic ring artifact, and translation compensation.
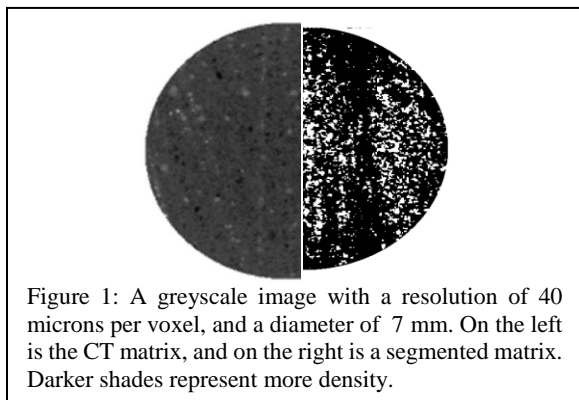
Figure 1: A greyscale image with a resolution of 40 microns per voxel, and a diameter of 7 mm. On the left is the CT matrix, and on the right is a segmented matrix. Darker shades represent more density.

Ultrasonic P wave speed was measured at 2426 m/s on a larger sample, extracted from the same block of rock. The transmission pulse method was used at room pressure and temperature, at a frequency of ~1 MHz (Birch, 1961). The sample porosity was measured by means of a helium pycnometer and was 21.5%. The rock sample density was 2056 kg/m^3.

The model was processed using three different methods. First, the average density and porosity for the entire rock were plugged into EMTs models. This was used to solve for effective bulk and shear moduli, and finally effective P wave velocity. The second and third method involved digital rock physics: by using segmentation, and then the segmentation-less—approach. A simulated wave was propagated through these models. Segmentation-less DRP (the third method) was performed for multiple EMTs to compare effectiveness.

Segmentation:

As the rock makeup is known to be ~95% quartz (Lai at al., 2014; Kareem et al., 2017), high attenuating voxels can be assigned the property of quartz, and low attenuating voxels can be assigned a value for air. Given that porosity is known at 21.5%, the 78.5% of voxels with the highest attenuation values were assigned the properties of quartz, and the remaining were assigned the value for air. Density, porosity, and stiffness matrices are created by giving the assigned voxels the quartz and air values seen in Table 1.

Table 1: Segmentation values quartz and air matrices.

	Density, ρ (kg/m^3)	Porosity, φ	Bulk Modulus, K (GPa)	Shear Modulus, G (GPa)
Quartz	2650	0	36	44
Air	1	1	0.0001	0

Segmentation-less method:

In order to calibrate the segmentation-less approach, the sample was acquired along with targets of known density. Target voxels were clustered by location to create averages for air, steel, and the sample rock. The average value for air was subtracted from every voxel, thereby normalizing all voxels to zero density (Table 2).

Table 2: Inputs for the calibration curve.

	Density, ρ (kg/m^3)	CT number
air	1	0
entire sample	2056	481
steel holder	8100	7042

A three point calibration conversion curve could then be made with the data from table 2:

$$Density_{voxel}(kg/m^3) = 87.66(CTnumber)^{0.511} \qquad (1)$$

The porosity conversion is equation 2, which is a linear relationship where densities of 2650 have porosities of 0, and densities of 0 have porosities of 1. For reference, 1.5% of the total voxels had values greater than 2650, which were then assigned the 'ceiling value' of 2650.

Choosing an Effective Medium for Digital Rock Physics with Micro Computed Tomography

$$Porosity_{voxel} = -0.000375 Density_{voxel} + 1 \qquad (2)$$
$$Where: Density_{voxel} > 2650 \rightarrow Density_{voxel} = 2650$$

Next, voxels need to be assigned moduli of bulk and shear. We employ two EMTs: The first is the Modified Hashin-Shtrikman bound with varying critical porosities to calculate different stiffness matrices. Equations 3 and 4 were applied to each voxel to assign its respective bulk and shear modulus (Nur et a., 1998):

$$K_{voxel} = K_{qz} + \frac{\frac{\phi_{voxel}}{\phi_C}}{\left(K_{air}-K_{qz}\right)^{-1}+\frac{(1-\frac{\phi_{voxel}}{\phi_C})}{K_{qz}+\frac{4}{3}G_{qz}}} \qquad (3)$$

$$G_{voxel} = G_{qz} + \frac{\frac{\phi_{voxel}}{\phi_C}}{\left(G_{air}-K_{qz}\right)^{-1}+\frac{2\left(1-\frac{\phi_{voxel}}{\phi_C}\right)}{\frac{K_{air}+2\,G_{qz}}{5G_{qz}(K_{qz}+\frac{4}{3}G_{qz})}}} \qquad (4)$$

Where K_{qz} K_{air} G_{qz} and G_{air} represent bulk and shear moduli of the quartz and air members specified (values in Table 1). Φ_{voxel} is the porosity of the voxel, and ϕ_C is the critical porosity.

In variation of MHS and to understand the sensitivity of the segmentation-less method, stiffness matrices were calculated using the Voigt-Reuss-Hill (VRH) bound (Hill,1952). Additionally, VRH was modified similarly to the MHS bound, i.e., by introducing the critical porosity. Modified VRH bounds (MVRH) are defined as:

$$K_{voxel} = \frac{\left[\left(K_{qz}\left(1-\frac{\phi_{voxel}}{\phi_C}\right)+K_a\frac{\phi_{voxel}}{\phi_C}\right)+\left(\frac{1-\frac{\phi_{voxel}}{\phi_C}}{K_{qz}}+\frac{\frac{\phi_{voxel}}{\phi_C}}{K_{air}}\right)^{-1}\right]}{2} \qquad (5)$$

$$G_{voxel} = \frac{\left[\left(G_{qz}\left(1-\frac{\phi_{voxel}}{\phi_C}\right)+G_{air}\frac{\phi_{voxel}}{\phi_C}\right)+\left(\frac{1-\frac{\phi_{voxel}}{\phi_C}}{G_{qz}}+\frac{\frac{\phi_{voxel}}{\phi_C}}{G_{air}}\right)^{-1}\right]}{2} \qquad (6)$$

For both MHS and MVRH, Voxels with ϕ_{voxel} greater than ϕ_C are set to equal ϕ_C. Critical porosity values are not well defined, and according to the literature tend to range between ~36% and 40% depending on the maturity of the rock (Nur et al., 1998).

To test the effect of different EMTs, MHS was experimented with critical porosities of 0.35, 0.375, and 0.40. VRH was applied, as well as MVRH with porosities of 0.35 and 0.40. These bounds are plotted in Figure 2, using equations 3 through 6.

Knowing stiffness and density, two 3D matrices can be made for V_p and V_s. At this stage, digital rock physics can be used to simulate the propagation of a wave through the rock. By picking a first arrival time from a simulated seismogram, an effective seismic velocity can be calculated. This was done

with SOFI3D, a three dimensional acoustic and viscoelastic seismic modeling software (Bohlen, 2002). SOFI used an eighth order finite difference, time explicit model in order to evaluate a simulated displacement at each node in three dimensions. A 1 MHz Ricker wavelet was used as a source function. Figure 3 shows snapshots depicting a propagating wave, and Figure 4 shows a synthetic recorded seismogram.
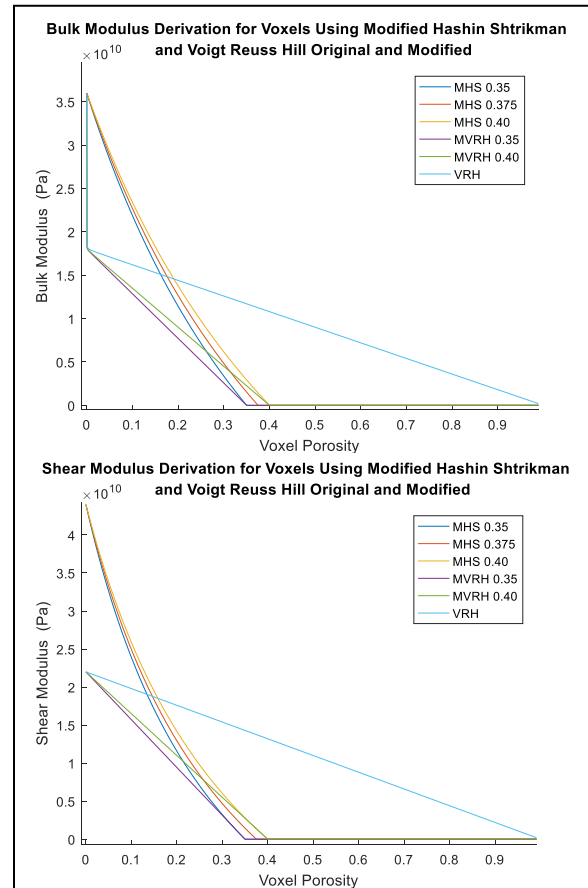
Figure 2: Bulk (above) and shear (below) moduli from equations 3 through 6. The curves are used for conversion between porosity and bulk and shear moduli.
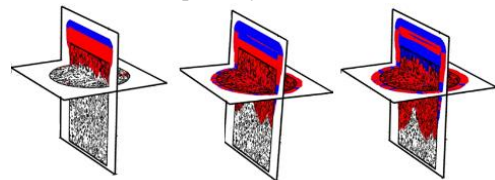
Figure 3: Synthetic renderings, showing slices of the three dimensional matrix with a wave propagating. The snapshots are taken at 1, 2.5, and 4 microseconds after the pulse was created. The scale for the cylinder shown is 15 mm long and 11.5 mm in diameter.

Choosing an Effective Medium for Digital Rock Physics with Micro Computed Tomography

Figure 4: A simulated seismogram, with a first arrival time picked to calculate V_p
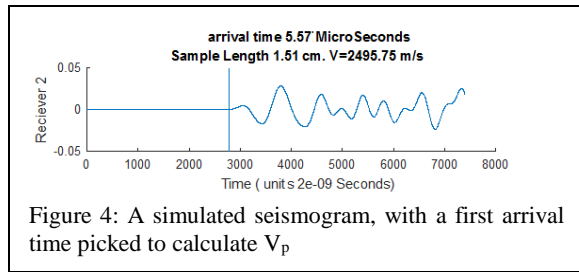
Results

Density and porosity from the segmentation-less method are within 2% and 12% of the laboratory measurements, respectively (calculated at 2017 kg/m^3 and 0.241). Density and porosity for the segmented method are not meaningful as they were used to calibrate the segmentation threshold.

Results from EMT calculations performed on the entire sample (i.e., simply applying EMTs to the whole sample), and results from ultrasonic wave propagation simulations can be seen in Figure 5. The following is a summary of the results:

1) No bound appears to be effective for the whole rock EMT. P wave velocity ranges from 2979 to 4251 m/s, or over predictions from 23% to 75%.
2) Segmentation based DRP performed poorly, providing a V_p of 3979 m/s, an error of 64%.
3) MVRH and VRH outputs V_p ranging between 2464 and 3221 m/s. This corresponds to error of 1.6 % and 33%. MVRH with a critical porosity of 35% is particularly effective.
4) MHS bounds outputs V_p ranging between 2882 m/s and 3053 m/s. This corresponds to error from 18% to 26%.

The segmented model over predicted the most of all the propagation models. This demonstrates a problem with traditional DRP and segmentation, and provides weight to the segmentation-less methods as a future tool for predictive DRP.

Fundamentally, MVRH yield lower elastic moduli than MHS. For both, stiffness will increase significantly as critical porosity increases incrementally (e.g., 1-2%). The highest moduli come from the VRH effective theory applied on the whole sample. These trends are identified in Figure 5, as V_p distance moves upwards in that sequence. The figure visually shows that the whole rock EMTs over predict V_p, whereas propagated simulations are far more accurate.

Some EMTs performed similarly to segmentation-less simulations. However, EMTs on whole samples disregard the internal distribution of stiffness that plays a role in the segmentation-less method. This is demonstrated by the fact that a given EMT, when applied to the whole sample, over predicts wave speeds compared to the corresponding segmentation less calculation (Figure 5).

Figure 5: V_p for each EMT normalized against the lab value (red star). Whole rock EMTs are squares, and propagated waves are circles. Both circles and squares have the same nature and parameters, but were calculated with different methods.
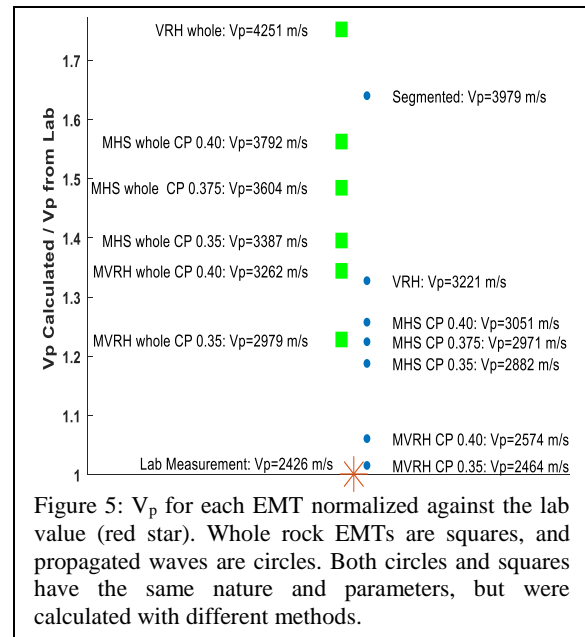
Conclusion

A segmentation-less method was successfully employed to estimate elastic properties of a Berea sandstone sample. The three dimensional propagation of an ultrasonic wave was accurate and effective. A MVRH bound with a critical porosity of 35% appears most effective for estimating P wave velocity correctly. A major benefit of the segmentation-less approach is that each voxel can be assigned non-binary properties to account for the effect of microscopic features that cannot be resolved by μCT. This potentially solves the issue with requiring very high resolutions for segmentation, and could allow decametric sized samples to be scanned without sacrificing quality of information gleaned. Testing more sandstones empirically may lead to a 'best practice' EMT, i.e. one that is ideal for the segmentation-less method. The selection of EMTs for specific lithologies would allow the method to be predictive, and not a 'fitting' excercise.

Acknowledgement

EDITED REFERENCES

Note: This reference list is a copyedited version of the reference list submitted by the author. Reference lists for the 2017 SEG Technical Program Expanded Abstracts have been copyedited so that references provided with the online metadata for each paper will achieve a high degree of linking to cited sources that appear on the Web.

REFERENCES

Andr, H., N. Combaret, J. Dvorkin, E. Glatt, J. Han, M. Kabel, Y. Keehm, F. Krzikalla, M. Lee, C. Madonna, M. Marsh, T. Mukerji, E. H. Saenger, R. Sain, N. Saxena, S. Ricker, A. Wiegmann, and X. Zhan. 2013, Digital rock physics benchmarks-part II: Computing effective properties: Computers & Geosciences, **50**, 33–43, https://doi.org/10.1016/j.cageo.2012.09.008.

Beer, A., 1852, Bestimmung der Absorption des rothen Lichts in farbigen Flüssigkeiten: Annalen der Physik und Chemie, **162**, 78–88, https://doi.org/10.1002/andp.18521620505.

Birch, F. 1961, The velocity of compressional waves in rocks to 10 kilobars: 2: Journal of Geophysical Research, **66**, 2199–2224, https://doi.org/10.1029/JZ066i007p02199.

Bohlen, T., 2002, Parallel 3-D viscoelastic finite difference seismic modelling: Computers & Geosciences, **28**, 887–899, https://doi.org/10.1016/S0098-3004(02)00006-7.

Catinat, M. 2010, Critical raw materials for the EU — Report of the Ad-Hoc working group on defining critical raw materials: EC.

Dunsmuir, J., S. Bennett, L. Fareria, A. Mingino, and M. Sansone, 2006, X-ray microtomographic imaging and analysis for basic research: Powder Diffraction, **21**, 125–131.

Dvorkin, J., J. Walls, A. Tutuncu, M. Prasad, A. Nur, and A. Mese, 2003, Rock property determination using digital rock physics: 73rd Annual International Meeting, SEG, Expanded Abstracts, 1660–1663.

Espinoza, D. N., I. Shovkun, O. Makni, and N. Lenoir, 2016, Natural and induced fractures in coal cores imaged through X-ray computed microtomography — Impact on desorption time: International Journal of Coal Geology, **154**, 165–175, https://doi.org/10.1016/j.coal.2015.12.012.

Hashin, Z., and S. Shtrikman, 1963, A variational approach to the theory of the elastic behaviour of multiphase materials: Journal of the Mechanics and Physics of Solids, **11**, 127–140, https://doi.org/10.1016/0022-5096(63)90060-7.

Hill, R., 1952, The elastic behaviour of a crystalline aggregate: Proceedings of the Physical Society, Section A, **65**, 349, https://doi.org/10.1088/0370-1298/65/5/307

Horsrud, P., 2001, Estimating mechanical properties of shale from empirical correlations: SPE Drilling & Completion, **16**, 68–73.

Kareem, R., P. Cubillas, J. Gluyas, L. Bowen, S. Hillier, and H. C. Greenwell, 2017, Multi-technique approach to the petrophysical characterization of Berea sandstone core plugs (Cleveland Quarries, USA): Journal of Petroleum Science and Engineering, **149**, 436–455, https://doi.org/10.1016/j.petrol.2016.09.029.

Ketcham, R. A., and W. D. Carlson, 2001, Acquisition, optimization and interpretation of X-ray computed tomographic imagery: Applications to the geosciences: Computers & Geosciences, **27**, 381–400, https://doi.org/10.1016/S0098-3004(00)00116-3.

Lai, P., and S. Krevor, 2014, Pore scale heterogeneity in the mineral distribution and surface area of Berea sandstone: Energy Procedia, **63**, 3582–3588, https://doi.org/10.1016/j.egypro.2014.11.388.

Landis, E. N., and D. T. Keane, 2010, X-ray microtomography: Materials Characterization, **61**, 1305–1316, https://doi.org/10.1016/j.matchar.2010.09.012.

Madonna, C., B. S. Almqvist, and E. H. Saenger, 2012, Digital rock physics: Numerical prediction of pressure-dependent ultrasonic velocities using micro-CT imaging: Geophysical Journal International, **189**, 1475–1482, https://doi.org/10.1111/j.1365-246X.2012.05437.x

Madonna, C., B. Quintal, M. Frehner, B. S. Almqvist, N. Tisato, M. Pistone, F. Marone, and E. H. Saenger, 2013, Synchrotron-based X-ray tomographic microscopy for rock physics investigations: Geophysics, **78**, no. 1, D53–D64, http://dx.doi.org/10.1190/geo2012-0113.1.

Marion, D., T. Mukerji, and G. Mavko, 1994, Scale effects on velocity dispersion: From ray to effective medium theories in stratified media: Geophysics, **59**, 1613–1619, http://dx.doi.org/10.1190/1.1443550.

Nur, A., G. Mavko, J. Dvorkin, and D. Galmudi, 1998, Critical porosity: A key to relating physical properties to porosity in rocks: The Leading Edge, **17**, 357–362, http://dx.doi.org/10.1190/1.1437977.

Tanaka, A., T. Nakano, and K. Ikehara, 2011, X-ray computerized tomography analysis and density estimation using a sediment core from the Challenger Mound area in the Porcupine Seabight, off Western Ireland: Earth, Planets and Space, **63**, 103–110, http://dx.doi.org/10.5047/eps.2010.12.006.

Taud, H., R. Martinez-Angeles, J. Parrot, and L. Hernandez-Escobedo, 2005, Porosity estimation method by X-ray computed tomography: Journal of Petroleum Science and Engineering, 47, no. 3, 209–217, https://doi.org/10.1016/j.petrol.2005.03.009.

Tisato, N., B. Quintal, S. Chapman, C. Madonna, S. Subramaniyan, M. Frehner, E. H. Saenger, and G. Grasselli, 2014, Seismic attenuation in partially saturated rocks: Recent advances and future directions: The Leading Edge, **33**, 640–646, http://dx.doi.org/10.1190/tle33060640.1.

Tisato, N., and K. Spikes. Computation of effective elastic properties from digital images without segmentation: 86th Annual International Meeting, SEG, Expanded Abstracts, 3256–3260, http://dx.doi.org/10.1190/segam2016-13947820.1.